AIP Advances

The impact of strain on growth mode in chemical vapor deposited mono- and few-layer MoS_2

Cite as: AIP Advances **12**, 065010 (2022); https://doi.org/10.1063/5.0087207
Submitted: 04 March 2022 • Accepted: 12 May 2022 • Published Online: 07 June 2022

Jonathan Rommelfangen, Sven Reichardt, Van Ben Chu, et al.

The impact of strain on growth mode in chemical vapor deposited mono- and few-layer MoS_2

Cite as: AIP Advances 12, 065010 (2022); doi: 10.1063/5.0087207
Submitted: 4 March 2022 • Accepted: 12 May 2022 •
Published Online: 7 June 2022

Jonathan Rommelfangen,[a] Sven Reichardt, Van Ben Chu, Ludger Wirtz, Phillip J. Dale, and Alex Redinger

AFFILIATIONS

Department of Physics and Materials Science, University of Luxembourg, Luxembourg, Luxembourg

[a]Author to whom correspondence should be addressed: jonathan.rommelfangen@uni.lu

ABSTRACT

-The development of high-quality chemical vapor-deposited mono- and few-layer MoS_2 is of high relevance for future applications in functional devices. Consequently, a detailed understanding of the growth mode and the parameters affecting it is important. Here, we show for the case of mono- and few-layer MoS_2 grown on Muscovite mica, how strain and temperature impact the growth mode. We show how misleading the determination of the number of MoS_2 layers is, solely based on Raman spectroscopy due to the occurrence of strain and changes in the growth mode. A combination of atomic force microscopy, Raman spectroscopy, and *ab initio* calculations reveal that that the growth at 500 °C synthesis temperature exhibits a strained layer-by-layer growth of up to three mono-layers, whereas at 700 °C, a strain release occurs and layer-by-layer growth is confined to the first mono-layer only. We relate the occurrence of strain to the formation of gas bubbles below the MoS_2 film, escaping the mica sheets during high temperature synthesis. Our analysis shows that mica substrates can be used to study strain in 2D materials without the need to apply external stress and that a detailed knowledge of the MoS_2 morphology is necessary to correctly interpret the Raman results.

I. INTRODUCTION

Since the discovery of graphene in 2004 by Geim and Novoselov,[1] the exploration of two dimensional materials (2D) began and revealed a huge variety of materials with unique properties and a wide range of applications.[2] Within the family of 2D materials, transition metal dichalcogenides (TMDs) with the general structural formula MX_2 are of particular interest. They are built up from a transition metal (M = Mo, W) and two chalcogenide (X = S, Se, or Te) atoms. Among them, MoS_2 is technologically very interesting due to its unique electronic[3] and optical properties,[4] leading to a large variety of suggested applications such as nanoelectronics,[5–7] solar cells,[8,9] and optoelectronics.[10,11] Particularly, for applications in future technologies, the realization of high-quality mono-layer (ML) and few-layer (FL) MoS_2 is crucial. To achieve high-quality ML or FL MoS_2, an atomically flat substrate is required. Therefore, Muscovite mica ($KAl_2[(OH,F)_2IAlSi_3O_{10}]$) is a well-suited substrate for growing 2D materials since it is an atomically flat and inert layered material that is easy to clean via cleaving.[12] Chae *et al.*[13] showed that a flat and chemically inert substrate decreases the amount of inherent strain and charge doping in the grown MoS_2 film. Advantageously, its mechanical flexibility allows us to investigate strain induced changes in the MoS_2 and other novel 2D materials.[14] Applying controlled strain to MoS_2 and other TMDs is interesting since it allows us to manipulate the electronic structure, e.g., a transition from direct to indirect bandgap can be observed.[15] To understand the observed electronic properties, the number of MoS_2 layers and the degree of strain must be known. In addition, the introduction of controlled strain, also unintended strain, can occur in the MoS_2 layer, for instance, in films grown via chemical vapor deposition (CVD).

The growth process for CVD-grown MoS_2, using metallic Mo as a precursor, on mica substrates is not well investigated yet, especially not from ML to FL MoS_2. For future applications where FL MoS_2 is needed, a proper understanding of its growth mode is

essential. In addition to the interest for the growth mode itself, being either Stranski–Krastanov (layer-plus-island growth; SK), Volmer–Weber (pure 3D island growth; VW), or Frank–van der Merwe growth (pure layer-by-layer growth; FM), it is also of interest in the case of SK-growth mode to find out what the critical layer thickness is and from where the transition from layer-by-layer to island growth occurs. Ji *et al.*[12] showed that for MoS_2 on mica grown at 530 °C, a Stranski–Krastanov (SK)-growth mode with a critical layer thickness of 1ML was observed, and they argued that compressive strain causes the transition from layer-by-layer to island growth. However, in that study, only ML MoS_2 with MoO_{3-x} as a precursor was grown. To determine quantities such as the number of MoS_2 layers or the critical layer thickness, several characterization techniques can be used. In the case of a fully covering film, the identification of the number of MoS_2 layers is usually carried out by employing Raman spectroscopy and identifying the peak distance between the high-frequency optical phonon modes A_{1g} and E^1_{2g},[12,16] which is also substrate dependent.[17,18] In the case of unstrained and atomically flat MoS_2 layers, this approach leads to unambiguous results. However, in the case of strained layers, the interpretation of the Raman spectra becomes more challenging since the strain in the MoS_2 will have a substantial impact on the position and peak distance of the high-frequency phonon modes. A tensile strain of only around 0.35% is already able to increase the peak distance by 0.5 cm^{-1}[19] while larger shifts in the range of several wavenumbers can be observed for compressive strain,[20] which is in the same range as the peak distance increase when going from ML to FL MoS_2.[4] This could lead to a wrong determination of the number of MoS_2 layers on fully covering MoS_2 films solely based on Raman spectroscopy. Hence, a proper understanding of how the high-frequency phonon modes are influenced by strain is crucial. Furthermore, strain effects need to be decoupled from morphological effects (roughness, layer number, growth mode). A simple example illustrates the impact of the morphology. A completely flat fully covering bi-layer exhibits, according to density functional theory (DFT) calculations, a Raman peak distance of 23 cm^{-1}. In the case of an SK-growth mode with a critical layer thickness of 1ML, it could be envisioned as half of the area being covered with 1ML of MoS_2 and the rest with tri-layer MoS_2. Here, we then assume that the tri-layer structures are small enough and evenly distributed on the surface such that the laser spot size, with a usual diameter of 1 μm, always measures an area such that 50% of the signal is coming from the mono-layer and 50% from the tri-layer MoS_2. Hence, the Raman peak separation would result in $0.5 \times 20 + 0.5 \times 24 = 22$ cm^{-1} where we assume a thickness independent Raman yield, and a peak separation of 20 cm^{-1} for ML and 24 cm^{-1} for tri-layer MoS_2. Consequently, redistributing a bi-layer of MoS_2 to a monolayer with 50% coverage of a tri-layer results in a change of the Raman peak separation by 1 cm^{-1}. This simple thought experiment highlights that the analysis of FL MoS_2 by Raman spectroscopy always needs to be accompanied by a nanoscale analysis of the morphology.

In this study, we investigate the growth mode of MoS_2 on Muscovite mica sheets in order to better understand the interplay between the film thickness, strain, and growth mode. We show how misleading the determination of the number of MoS_2 layers is, solely based on Raman spectroscopy due to the occurrence of strain and different growth modes, which is corroborated by DFT calculations. We also show that the layer-by-layer growth of CVD-grown ML to FL MoS_2 films on mica depends sensitively on the substrate temperature. This can be traced back to the thermal expansion of different amounts of encapsulated gases dissolved in the mica sheets, which changes the strain in the 2D layer during the sulfurization. Our analysis shows that mica substrates can be used to study strain in 2D materials, without the need to apply external stress and that the growth mode needs to be studied with atomic force microscopy (AFM) in combination with Raman spectroscopy to disentangle the different contributions that impact the Raman peak separation.

II. METHODS

The thickness of the metallic Molybdenum (Mo) film varied between 0.18 and 1.8 nm followed by a sulfurization in a tube furnace. The deposition of metallic Mo was carried out by DC sputtering, with a sputter rate of 0.18 nm/s at 240 W. The sputter rate was calibrated via a quartz crystal monitor. Two thickness sets were sulfurized at 500 and 700 °C for 30 min each. All sulfurizations were made with the same and constant heating ramp. For this, the Mo covered mica sheets were placed in a graphite box together with elemental sulfur. From the thickness of the sputtered Mo film (h_{Mo}), it is possible to estimate the number of fully covering MoS_2 ML equivalents (MLE) that can grow from it, by linking h_{Mo} to the MoS_2 film thickness (h_{MoS_2}). The details are explained in the supplementary material, and the final relation is described by $h_{MoS_2} = 3.4 \times h_{Mo}$. Hence for growing one fully covering ML of MoS_2 (N_{tot} = 1MLE), one needs to sputter 0.18 nm of metallic Mo, with the height of one ML of MoS_2 being 0.65 nm. The total amount of deposited MoS_2 deduced from this relation is referred to as N_{tot} in the following. For thicker films, this procedure can be easily scaled up and controlled via the Mo deposition time. The actual amount of grown MoS_2 was corroborated via ambient AFM and analyzed via gray scale determination. From the topographies acquired via AFM, the number of open MoS_2 layers, N_{OL}, was deduced by applying a height threshold in steps of 0.65 nm (height of an ML of MoS_2). N_{OL} does not necessarily coincide with the total number of layers, since in AFM, we cannot estimate the number of fully covering layers below the islands. Retrieving the area A_i of each open layer yields a histogram of A_i against N_{OL}. Summing them up yields the number of fully covering MoS_2 ML equivalents, N_{MLE}, that the MoS_2 in the open layers correspond to, expressed as

$$N_{MLE} = \sum_{i=1}^{N} \frac{A_i}{A_{tot}} \times 1\,\text{ML}. \quad (1)$$

N is limited by the condition that the area A_i of an open layer at a height step of i must be larger than zero. The value for N_{MLE} is calculated by taking the sum over all open layers N from all the relative ratios of the area A_i of the open layer i and the total area of the topography A_{tot}, being 10×10 μm^2, and multiplying it with 1 ML. By definition, the amount of hidden MoS_2 layers, N_{hidden}, that are invisible for the AFM, is deduced by subtracting the amount of

MoS_2 contained in the open layers, N_{MLE}, from the total deposited number of ML MoS_2, N_{tot} [Eq. (2)],

$$N_{hidden} = N_{tot} - N_{MLE}. \quad (2)$$

The AFM measurements were performed with the MultiMode AFM with Nanoscope V controller in tapping mode. The AFM measurements were carried out under ambient conditions, e.g., the samples were air exposed. The Raman spectra were acquired with a Renishaw inVia spectrometer at ambient conditions with a 442 nm laser, a 2400 $\frac{1}{mm}$ grating, and a power of 277 μW that did not damage our sample. The peak fitting for the high-frequency optical phonon modes E^1_{2g} and A_{1g} turned out to be challenging due to an overlap with the underlying mica Raman modes, which is further elaborated in the supplementary material, Fig. S1. When comparing the FWHM of the Raman peaks of the high-frequency phonon modes A_{1g} and E^1_{2g} of a bulk single crystal of MoS_2 with those from the CVD grown 5ML 500 °C and 5ML 700 °C samples (see supplementary material, Fig. S8), it is clear that the latter two show broader peaks. This is further discussed in the supplementary material.

We realized in this work that PL is not a suitable tool to measure the optical qualities of the MoS_2 film, since the PL of mica is very dominant and interferes with the PL of MoS_2. The PL measurements are displayed in the supplementary material, Fig. S6.

For the first-principles calculations of the phonons of strained mono-layer and bulk MoS_2, we employed density functional perturbation theory (DFPT) as implemented in the QuantumESPRESSO suite.[21,22] We use optimized, norm-conserving Vanderbilt pseudopotentials[23] to describe the bare electron–nuclei interaction, explicitly retaining the molybdenum semi-core 4*s* and 4*p* states in the set of valence electrons. The electron–electron interaction was approximated on the level of the local density approximation (LDA) in the parametrization of Perdew and Wang.[24] The electronic wave functions were expanded in a plane wave basis, using an energy cutoff of 120 Ry. We sampled the first Brillouin zone of mono-layer MoS_2 with a 12 × 12 × 1 uniform mesh, while we used a 12 × 12 × 4 uniform mesh for bulk MoS_2.

For both the mono-layer and bulk case, we first obtained the relaxed crystal structure and optimized the nuclei positions in the unstrained case. The total energy was converged up to 10^{-7} Ry, each component of the residual force on each atom was required to be less than 10^{-8} Ry/bohr, and the total pressure was required to be less than 0.02 kbar in the relaxed structure. In the case of mono-layer MoS_2, we only relaxed the in-plane lattice constant, finding a value of 3.121 Å, using a vacuum spacing (Mo–Mo distance) of 16 Å to avoid spurious interactions between layers. For bulk MoS_2, we relaxed both the in- and out-of-place lattice constants, finding relaxed values of 3.123 and 12.074 Å, respectively.

We then performed calculations with in-plane biaxial strain by varying the in-plane lattice constant. In each case, we optimized the nuclei positions in the strained structure. For bulk MoS_2, we additionally re-calculated the optimized out-of-plane lattice constant in the strained geometry.

Finally, we performed a DFPT calculation for every optimized structure to obtain the zero-momentum phonons. The change in the self-consistent potential was converged up to 10^{-14} Ry/bohr. We also applied an acoustic sum rule correction to the force constants to ensure that the acoustic phonon branches have zero frequency.

III. EXPERIMENTAL RESULTS

Figure 1 shows representative AFM topography images of a thickness series of MoS_2 films grown on mica for two different sulfurization temperatures, 500 °C [Figs. 1(a)–1(c)] and 700 °C [Figs. 1(d)–1(f)]. As discussed in Sec. II, the thickness of the MoS_2 film was controlled by the precursor Mo film thickness. In Fig. 1(a), approximately N_{tot} = 1MLE of MoS_2 was deposited on mica. Gray scale discrimination, as outlined in the methods section of the AFM topography images, was carried out in order to cross-check the amount of MoS_2 and to study the growth mode. From the analysis

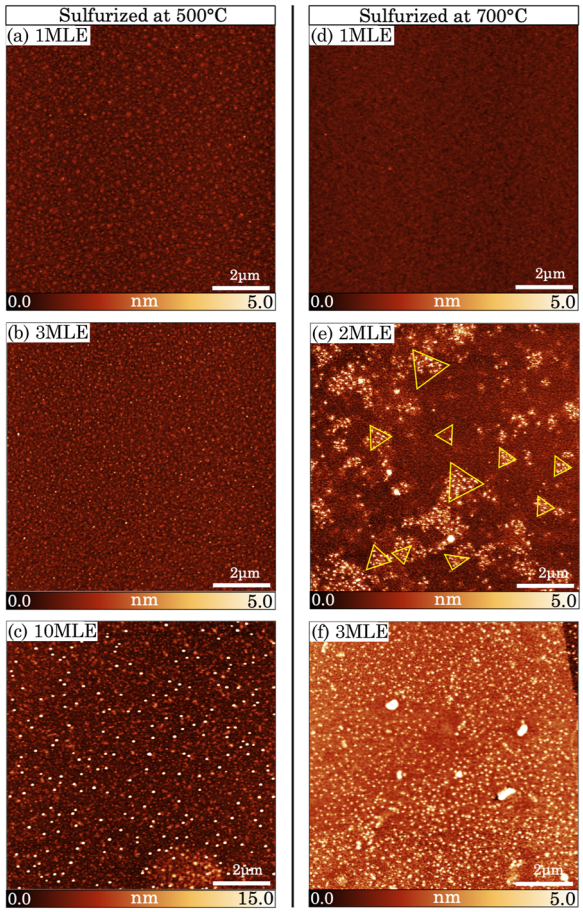

FIG. 1. AFM topography images for different thicknesses of MoS_2 films grown on mica for two different sulfurization temperatures for the (a)–(c) 500 °C and (d)–(f) 700 °C sulfurization. The height scale is adjusted for maximum contrast and depicted below each image. (e) Preferential nucleation on bi-layer flakes as indicated by the yellow triangles. A different growth mode is observed for the two sulfurization temperatures. All AFM images are shown in the supplementary material, Fig. S5.

of Fig. 1(a), we deduced one almost fully covering MoS_2 layer (90%) and ~10% coverage of a second layer, i.e., $N_{MLE} = N_{tot} = 1$ MLE of MoS_2, in excellent agreement with the estimated MoS_2 thickness deduced from the sputtering rate calibration. Line scans across the surface corroborated that the height of the small grains is in accordance with the height of one ML of MoS_2 being 0.65(±0.1) nm. The grain size is rather small with a lateral extension of 100 nm, neglecting artifacts due to the finite size of the AFM tip. The situation did not change much after a threefold increase in the initial Mo amount, as we observed only two open layers with a distribution of ~90% and 10%, corresponding to an amount of one ML of MoS_2. The remaining amount is contained in two underlying fully covering ML of MoS_2, which are not visible in the AFM topography images. We also observed for the 3 MLE sample the formation of small islands, visible as tiny white dots in the topography in Fig. 1(b). However, layer-by-layer growth is still the dominating growth mode. Only for the 10 MLE of MoS_2, we observe the formation of large island structures, which is corroborated by gray scale discrimination of the AFM images, where the number of open layers increased. This clearly shows that the growth mode changed, and for the case of 10 MLE of MoS_2, we observed an average $N_{MLE} = 3$ MLE open layer equivalents. However, the individual islands were much higher and we measured structures with up to $N_{OL} = 23$ open layers.

By definition, the total deposited number of MLE of MoS_2, N_{tot}, is given by the sum of the amount of MoS_2 in open layers, N_{MLE}, and in hidden layers, N_{hidden}, [Eq. (2)]. For the 500 °C 10 MLE case, we found $N_{MLE} = 3$ MLE and $N_{hidden} = 7$ MLE. This analysis was repeated for all MoS_2 thicknesses and summarized in Fig. 2(a). We observed that the amount of MoS_2 included in those island structures is with 3 MLE substantially enlarged for the $N_{tot} = 10$ MLE sample, while for the $N_{tot} = 3$ MLE and 5 MLE samples, N_{MLE} values of 1.1 resp. 1.4 MLE were deduced. From this analysis, we could identify a clear transition from $N_{MLE} \approx 1$, indicative of layer-by-layer growth, to $N_{MLE} > 1$ MLE, which is typical for 3D growth modes. The physical reason for this change in growth mode will be discussed later in the manuscript. We would like to first discuss the temperature dependence of the growth mode by analyzing the samples sulfurized at 700 °C.

In contrast to 500 °C, where solely layer-by-layer growth of up to $N_{tot} = 5$ MLE was observed, the samples sulfurized at 700 °C showed a transition to a 3D-growth mode for lower amounts of Mo precursor, as shown in Figs. 1(d)–1(f) and 2(b). The $N_{tot} = 1$ MLE MoS_2 film is still similar to the 500 °C case with only two open layers with ~95% and 5% coverage. However, already at $N_{tot} = 2$ MLE, we observed a substantial roughening and a clear transition to a 3D-growth mode with some preferential nucleation in specific regions on the surface [triangles in Fig. 1(e)]. Some of these regions exhibited a triangular shape, which we related to the extension of the MoS_2 flake beneath. This enhanced nucleation only took place on bi-layer islands. Next, for $N_{tot} = 3$ MLE, the nucleation was present on the whole surface [Fig. 1(f)]. In contrast to 500 °C, the $N_{tot} = 10$ MLE sample sulfurized at 700 °C showed with $N_{MLE} \approx 8$ MLE a substantially larger amount of material contained in island structures. The summary of the analysis of the MoS_2 growth at 700 °C is depicted in Fig. 2(b). The graph confirms the enhanced island growth observed at 700 °C compared to 500 °C. The decreased critical layer thickness, being only one fully covering ML,

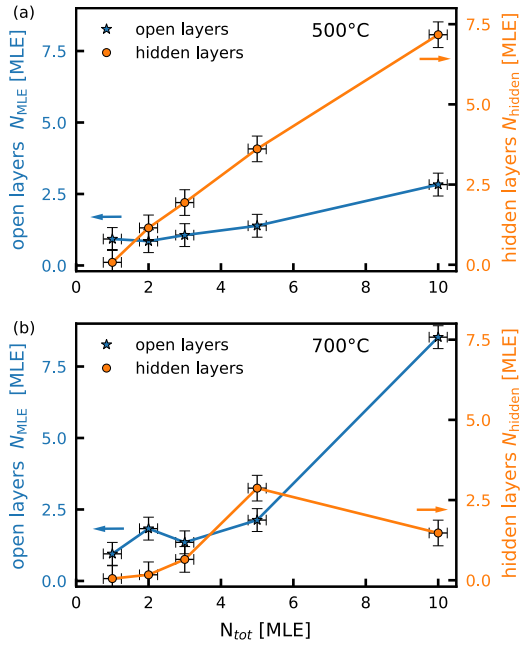

FIG. 2. Coverage of MoS_2 on the mica substrate in height steps of an ML (0.65 nm) for the (a) 500 °C and (b) 700 °C series. The total amount of grown MoS_2, N_{tot}, is deduced from the deposition rate, and the amount of open layer equivalent, N_{MLE}, deduced via Eq. (2), is shown on the left hand axis. The number of fully covering hidden layers, N_{hidden}, is deduced from Eq. (2) and depicted on the right hand axis.

for the 700 °C set, cannot be explained solely by the AFM measurements. Thus, Raman analysis is necessary, which will be discussed in the following.

Before, we like to discuss briefly if the 700 °C films suffered from a partial thermal desorption of MoS_2. The 10 MLE sample exhibited a uniform Raman signal, which excludes a complete dewetting of the film. Since we measured approximately $N_{MLE} = 8$ MLE and we need to assume that there is at least one fully covering ML of MoS_2 present everywhere on the surface, we can estimate that maximally 1 MLE could have been lost during the synthesis (assuming a deposition of 10 MLE in total). Consequently, the desorption of Mo-species in large quantities is not probable and will be neglected in the following.

Figure 3 summarizes the Raman analysis carried out on the sample series presented before. The left hand axis depicts the Raman peak distance d measured between the E^1_{2g} and A_{1g} modes, which allows us to estimate the film thickness. The right hand axis depicts the individual high-frequency optical phonon modes E^1_{2g} and A_{1g} for both temperature series as a function of N_{tot} in order to be independent of the growth mode. For FM growth, N_{tot} is analogous to the film thickness due to the layer-by-layer growth. However, this is not the case for SK growth, where a detailed analysis of the morphology is crucial. As discussed before in the introduction, it is important how the height, diameter, and nucleation density of the island structures behave with respect to the laser spot diameter. In this case, we averaged the signals coming from the hidden layers and the island structures based on the parameters such as height, diameter, and

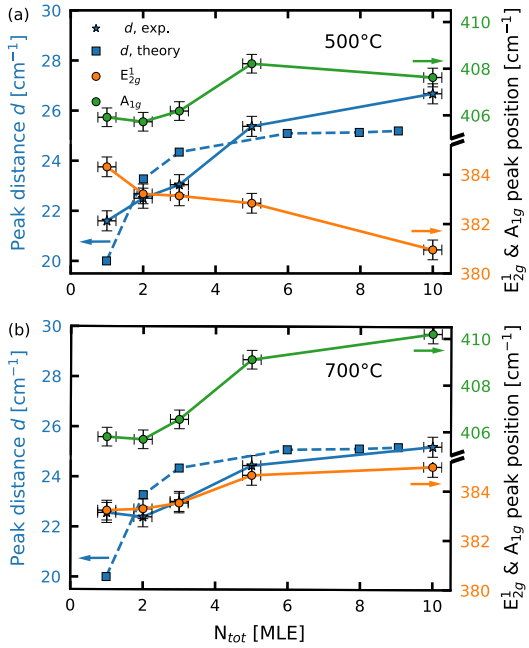

FIG. 3. Raman measurements of MoS_2 on mica for the (a) 500 °C and (b) 700 °C series. Both graphs display the individual peak positions of the E^1_{2g} (orange) and A_{1g} (green) modes as well as their peak distance *d* (blue). The experimental values are compared to the theoretical values displayed as dashed lines (for details, see the text).

coverage. For the latter, we assumed based on the height, which is larger than six stacked ML of MoS_2, bulk properties in terms of the peak distance between the E^1_{2g} and A_{1g} modes.

For example, the 700 °C 3 MLE sample showed that N_{MLE} [Fig. 2(b)] represented to a significant portion the bulky islands on top of two fully covering MoS_2 ML [see Fig. 1(b)]. Therefore, the Raman signal will be averaged between the two fully covering ML and the bulky island. However, in this case, the island structures are sparsely distributed such that the peak distance deduced from the E^1_{2g} and A_{1g} modes are mainly influenced by the two fully covering ML. For the series sulfurized at 500 °C, displayed in Fig. 3(a), the A_{1g} mode is blue-shifted by 2 cm^{-1} from 1 MLE to 10 MLE. The E^1_{2g} mode is red-shifted by ~3 cm^{-1} with increasing number of MoS_2 layers. This trend is known from the literature[4] and arises from a smaller force constant for neighboring S–Mo bonds in bulk, due to more screening from the surrounding MoS_2 layers, thus leading to a red-shift for the E^1_{2g} mode,[25] and additional springs in the form of inter-layer van der Waals bonds leading to an increased restoring force and, therefore, to a blue-shift for the A_{1g} mode from ML to bulk MoS_2.[26] When the peak positions and their spacing, i.e., peak distance *d*, are compared with those from the literature,[4,26] both modes are red-shifted and their spacing is enlarged by 1.5 cm^{-1} for the 1 MLE and 10 MLE samples and by 1 cm^{-1} for the 5 MLE sample. In Figs. 3(a) and 3(b), we included the theoretical values of *d* from Molina-Sánchez *et al.*[26] This indicated that for MoS_2 grown at 500 °C, tensile strain was present.

Tensile strain causes a red-shift of both high-frequency phonon modes, due to a decrease in the force constant caused by a lengthened intra-layer bond between the S and Mo atoms, which has a stronger influence on the in-plane E^1_{2g} mode compared to the out-of-plane A_{1g} mode, leading as well to an increase in the peak distance between these two modes. The red-shift of the high-frequency optical phonon modes is well known from the literature.[19,27] The sample set sulfurized at 700 °C, displayed in Fig. 3(b), shows a different trend. The position of the E^1_{2g} mode is constant between the 1 and 3 MLE samples followed by a blue-shift contrasting the 500 °C series. The peak position of the A_{1g} mode is also constant until the 2 MLE sample. Starting from the 3 MLE sample, it is blue-shifting by 1 cm^{-1}. Starting from the 5 MLE sample, it is strongly blue-shifting by 3 cm^{-1}. The peak distance of the 1 MLE sample is enlarged by 2.5 cm^{-1}, indicating an increased tensile strain compared to the 500 °C 1 MLE sample. For the 2 MLE sample, the peak distance stays constant, which is explained by the fact that the island growth is enhanced and very selective, i.e., on bi-layer flakes, leaving large open patches of up to 3 μm in diameter, where only the fully covering ML of MoS_2 is visible. Hence, when measuring Raman spectroscopy with a spot size of 1 μm in diameter, the main signal is characterized by this ML. For the 3 MLE sample, as previously explained, the Raman signal and, therefore, also the peak distance are mainly influenced by the two fully covering ML. Hence, the peak distance is reduced and similar to the theoretical value for 2 MLE MoS_2. For the 700 °C 5 MLE and 10 MLE samples, the peak distance shows the same values as expected theoretically, indicating that the tensile strain observed in the 700 °C 1 MLE and 2 MLE samples is released.

An important outcome of the Raman analysis is that the peak distance is not a good measure for the MoS_2 film thickness. In both cases (500 and 700 °C), we observed an increase in the peak separation as a function of N_{tot}, in accordance with the literature. However, the exact values differ substantially and a reliable measurement of the film thickness via Raman spectroscopy was not possible for the present set of samples. The physical reason for this discrepancy will be discussed in the following in more detail. Raman measurements indicate that some of the films are strained. To illustrate and better understand the effect of strain on MoS_2 film thickness and synthesis temperature, DFT calculations were carried out for ML and bulk MoS_2 as depicted in Fig. 4 (for details, see Sec. II).

We focus on the peak separation only, since this can be estimated reliably from DFT in the commonly used LDA, whereas the phonon frequencies (i.e., the exact Raman shift or peak positions of the E^1_{2g} and A_{1g} modes) for covalently bonded semiconductors tend to be overestimated in the LDA. The simulated values of the peak positions can be found in the supplementary material. From Fig. 4, we see that the Raman peak separation increases for the case of tensile strain, which is what we observed for many of our samples. For the case of 500 °C, we do measure peak separations, which are compatible with ~0.8% tensile strain in the films. We stress that the exact value of the strain deduced by DFT may be slightly different. We will use the theoretical values in the following to discuss trends only. We assume the slight estimated decrease in strain between the ML and bulk values to be within the error of the measurement. The 700 °C samples were different. The Raman peak separation was compatible with strain values exceeding 1% in the case of 1 MLE of MoS_2, which strongly dropped in the bulk samples. Consequently, the samples grown at 500 °C

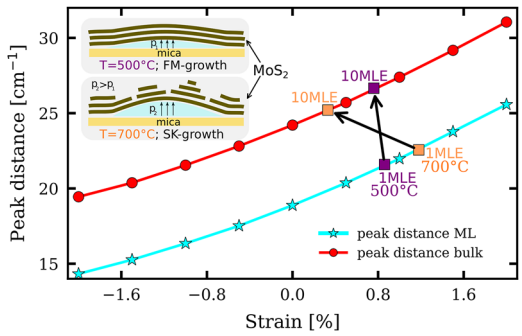

FIG. 4. Impact of strain on Raman peak distance *d* as calculated via DFT simulations. The experimentally measured peak distances for 1 MLE and 10 MLE are highlighted on top of the simulation data for 700 °C (orange) and 500 °C (purple). For 700 °C, a strain release is observed, while the strain for the 500 °C set is almost unchanged. The inset schematically shows the proposed model. Expansion of encapsulated gases between the layered mica sheets leads to strain in MoS_2. The expansion is temperature dependent [p_2 (at 700 °C) > p_1 (at 500 °C)]. The increased tensile strain at 700 °C compared to 500 °C causes a transition from an FM- to an SK-growth mode after a critical layer thickness of only 1 MLE. At 500 °C, samples grow in FM-mode until 3 MLE. The transition in growth mode causes a partial strain release in the MoS_2 film, as indicated by the arrows in the simulation data.

have a constant strain, whereas the samples at 700 °C exhibit a strain release.

The inset in Fig. 4 schematically shows how we interpret the data. It is well known that in Muscovite mica, gas and water molecules are intercalated between mica sheets.[28] The MoS_2 layer on top of the mica acts as an impermeable barrier, which confines the gas to a finite volume, similar to graphene.[29] An increase in temperature leads to a large increase in pressure of the confined gas, which ultimately leads to strain in the MoS_2 sheets. Strain is known to impact the growth of thin layers during heteroepitaxy.[30] In the present case, strain is not dictated by a lattice mismatch directly (van der Waals epitaxy) but due to the encapsulated gas below the MoS_2 during high-temperature synthesis. The pressure and consequently the strain are higher for the 700 °C films, compared to the ones grown at 500 °C. The Raman measurements of the 1 MLE of MoS_2 films corroborate this hypothesis. The Raman peak distance for the sample with 1 MLE of MoS_2 at 700 °C is larger than for 500 °C, as indicated in Fig. 4.

The increased amount of strain at higher synthesis temperatures induced a change in growth mode. It is known theoretically and experimentally that strain may change the diffusion and nucleation processes during thin film growth.[31,32] Our AFM data [Fig. 1(e)] showed a high nucleation density in the third layer, indicating that at 700 °C, the kinetics of film formation was different than at 500 °C. As a consequence, we observe a faster change to an SK-growth mode at 700 °C, compared to 500 °C. The thicker layers are also well in accordance with our proposed model, where the peak distance of the 700 °C films is very close to the theoretical value of unstrained material, whereas the 500 °C films still show similar strain values as the ML films. To prove that there is gas encapsulated within the mica sheets, we used mica covered with 200 nm of Au and flame-annealed these layers in air. After annealing, we observed the formation of bulges that arose from the encapsulated gas that expanded and therefore strained the Au layers. At 700 °C, the pressure was so high that the Au film cracked in specific regions. This experiment, which is shown in the supplementary material, unambiguously showed that the encapsulated gas can, in fact, change the strain in thin films grown on mica.

IV. CONCLUSION

The difference in growth mode is caused by tensile strain in the MoS_2 film due to the encapsulated gasarising from the Muscovite mica substrate below the MoS_2 during high temperature synthesis. The tensile strain causes a red-shift in the high-frequency optical phonon mode positions as well as an increased peak distance between them. The simulations show that for the 700 °C set, a strain release can be observed for the 3, 5, and 10 MLE samples, while for the 500 °C, no strain release is observed. Future applications of 2D materials in optoelectronic devices require large area synthesis on different substrates with different lattice constants. Our work highlights that Raman measurements alone are certainly not suitable to give reliable information on the film thickness when strain is involved during growth. This result is well supported by detailed Raman measurements of exfoliated 2D materials under strain. Most importantly, the growth mode and the nucleation kinetics are also impacted, which requires a detailed understanding of the growth mode for the case where FL 2D materials need to be synthesized. Finally, the mica substrate offers an ideal playground to study strain effects in 2D materials. This includes studies as shown here but could also be extended to exfoliated material systems.

SUPPLEMENTARY MATERIAL

See the supplementary material for the estimation of the total amount of grown MoS_2 (N_{tot}), the treatment of the Raman spectra (Fig. S1), all Raman spectra (Fig. S2), all the phonon frequencies from DFT calculations (Fig. S3), the influence of flame annealing on Gold covered mica (Fig. S4), all AFM topographies (Fig. S5), the PL measurements (Fig. S6), the influence of sulfurization on bare mica (Fig. S7), the FWHM of the Raman peaks (Fig. S8), and the Raman mappings (Fig. S9).

ACKNOWLEDGMENTS

We thank Dr. Michele Melchiorre for Mo sputtering, Daniel Siopa for the sulfurizations, Evandro Lanzoni for AFM training and useful discussions, and Dr. Ulrich Siegel and Dr. Bernd Uder for the technical support. The authors acknowledge funding from the Fonds National de la Recherche Luxembourg (FNR). A.R. acknowledges funding from the FNR project "Sunspot" (Grant No. 11244141). P.D. acknowledges funding from the FNR project "Starsol" (Grant No. C18/MS/12686759). S.R. acknowledges funding from the FNR project "RESRAMAN" (Grant No. C20/MS/14802965). L.W. acknowledges funding from the FNR project "Accept" (Grant No. INTER/19/ANR/13376969). J.R. acknowledges funding from the FNR project "AFR individuals" (Grant No. 13584473).

AUTHOR DECLARATIONS

Conflict of Interest

The authors have no conflicts to disclose.

DATA AVAILABILITY

The data that support the findings of this study are available within the article and its supplementary material.

REFERENCES

[1] K. S. Novoselov, A. K. Geim, S. V. Morozov, D. Jiang, Y. Zhang, S. V. Dubonos, I. V. Grigorieva, and A. A. Firsov, "Electric field effect in atomically thin carbon films," Science **306**, 666–669 (2004).

[2] W. Choi, N. Choudhary, G. H. Han, J. Park, D. Akinwande, and Y. H. Lee, "Recent development of two-dimensional transition metal dichalcogenides and their applications," Mater. Today **20**, 116–130 (2017).

[3] A. Splendiani, L. Sun, Y. Zhang, T. Li, J. Kim, C.-Y. Chim, G. Galli, and F. Wang, "Emerging photoluminescence in monolayer MoS_2," Nano Lett. **10**, 1271–1275 (2010).

[4] C. Lee, H. Yan, L. E. Brus, T. F. Heinz, J. Hone, and S. Ryu, "Anomalous lattice vibrations of single- and few-layer MoS_2," ACS Nano **4**, 2695–2700 (2010).

[5] S. Wachter, D. K. Polyushkin, O. Bethge, and T. Mueller, "A microprocessor based on a two-dimensional semiconductor," Nat. Commun. **8**, 14948 (2016).

[6] H.-M. Li, D. Lee, D. Qu, X. Liu, J. Ryu, A. Seabaugh, and W. J. Yoo, "Ultimate thin vertical p-n junction composed of 2D layered molybdenum disulfide," Nat. Commun. **6**, 6564 (2015).

[7] P. K. Sahoo, S. Memaran, Y. Xin, L. Balicas, and H. R. Gutiérrez, "One-pot growth of two-dimensional lateral heterostructures via sequential edge-epitaxy," Nature **553**, 63–67 (2018).

[8] M.-l. Tsai, S.-H. Su, J.-K. Chang, D.-S. Tsai, C.-H. Chen, C.-I. Wu, L.-J. Li, L.-J. Chen, and J.-H. He, "Monolayer MoS_2 heterojunction solar cells," ACS Nano **8**, 8317–8322 (2014).

[9] M. Bernardi, M. Palummo, and J. C. Grossman, "Extraordinary sunlight absorption and one nanometer thick photovoltaics using two-dimensional monolayer materials," Nano Lett. **13**, 3664–3670 (2013).

[10] H. Wang, C. Li, P. Fang, Z. Zhang, and J. Z. Zhang, "Synthesis, properties, and optoelectronic applications of two-dimensional MoS_2 and MoS_2-based heterostructures," Chem. Soc. Rev. **47**, 6101–6127 (2018).

[11] N. Briggs, S. Subramanian, Z. Lin, X. Li, X. Zhang, K. Zhang, K. Xiao, D. Geohegan, R. Wallace, L.-Q. Chen, M. Terrones, A. Ebrahimi, S. Das, J. Redwing, C. Hinkle, K. Momeni, A. van Duin, V. Crespi, S. Kar, and J. A. Robinson, "A roadmap for electronic grade 2D materials," 2D Mater. **6**, 022001 (2019).

[12] Q. Ji, Y. Zhang, T. Gao, Y. Zhang, D. Ma, M. Liu, Y. Chen, X. Qiao, P.-H. Tan, M. Kan, J. Feng, Q. Sun, and Z. Liu, "Epitaxial monolayer MoS_2 on mica with novel photoluminescence," Nano Lett. **13**, 3870–3877 (2013).

[13] W. H. Chae, J. D. Cain, E. D. Hanson, A. A. Murthy, and V. P. Dravid, "Substrate-induced strain and charge doping in CVD-grown monolayer MoS_2," Appl. Phys. Lett. **111**, 143106 (2017).

[14] H. Lin, A. Rauf, N. Severin, I. M. Sokolov, and J. P. Rabe, "Influence of interface hydration on sliding of graphene and molybdenum-disulfide single-layers," J. Colloid Interface Sci. **540**, 142–147 (2019).

[15] H. J. Conley, B. Wang, J. I. Ziegler, R. F. Haglund, S. T. Pantelides, and K. I. Bolotin, "Bandgap engineering of strained monolayer and bilayer MoS_2," Nano Lett. **13**, 3626 (2013).

[16] M. A. Gonzalez, D. Pareek, L. Büsing, M. Beer, J. Parisi, S. Schäfer, and L. Gütay, "Rapid formation of large-area MoS_2 monolayers by a parameter resilient atomic layer deposition approach," APL Mater. **9**, 051122 (2021).

[17] A. Albagami, S. Ambardar, H. Hrim, P. K. Sahoo, Y. Emirov, H. R. Gutiérrez, and D. V. Voronine, "Tip-enhanced photoluminescence of freestanding lateral heterobubbles," ACS Appl. Mater. Interfaces **14**, 11006–11015 (2022).

[18] M. Buscema, G. A. Steele, H. S. J. van der Zant, and A. Castellanos-Gomez, "The effect of the substrate on the Raman and photoluminescence emission of single layer MoS_2," Nano Res. **7**, 561 (2013).

[19] H. Li, A. W. Contryman, X. Qian, S. M. Ardakani, Y. Gong, X. Wang, J. M. Weisse, C. H. Lee, J. Zhao, P. M. Ajayan, J. Li, H. C. Manoharan, and X. Zheng, "Optoelectronic crystal of artificial atoms in strain-textured molybdenum disulphide," Nat. Commun. **6**, 7381 (2015).

[20] G. Kukucska and J. Koltai, "Theoretical investigation of strain and doping on the Raman spectra of monolayer MoS_2," Phys. Status Solidi B **254**, 1700184 (2017).

[21] P. Giannozzi, S. Baroni, N. Bonini, M. Calandra, R. Car, C. Cavazzoni, D. Ceresoli, G. L. Chiarotti, M. Cococcioni, I. Dabo, A. Dal Corso, S. de Gironcoli, S. Fabris, G. Fratesi, R. Gebauer, U. Gerstmann, C. Gougoussis, A. Kokalj, M. Lazzeri, L. Martin-Samos, N. Marzari, F. Mauri, R. Mazzarello, S. Paolini, A. Pasquarello, L. Paulatto, C. Sbraccia, S. Scandolo, G. Sclauzero, A. P. Seitsonen, A. Smogunov, P. Umari, and R. M. Wentzcovitch, "QUANTUM ESPRESSO: A modular and open-source software project for quantum simulations of materials," J. Phys.: Condens. Matter **21**, 395502 (2009).

[22] P. Giannozzi, O. Andreussi, T. Brumme, O. Bunau, M. Buongiorno Nardelli, M. Calandra, R. Car, C. Cavazzoni, D. Ceresoli, M. Cococcioni, N. Colonna, I. Carnimeo, A. Dal Corso, S. de Gironcoli, P. Delugas, R. A. DiStasio, , Jr, A. Ferretti, A. Floris, G. Fratesi, G. Fugallo, R. Gebauer, U. Gerstmann, F. Giustino, T. Gorni, J. Jia, M. Kawamura, H.-Y. Ko, A. Kokalj, E. Küçükbenli, M. Lazzeri, M. Marsili, N. Marzari, F. Mauri, N. L. Nguyen, H.-V. Nguyen, A. Otero-de-la-Roza, L. Paulatto, S. Poncé, D. Rocca, R. Sabatini, B. Santra, M. Schlipf, A. P. Seitsonen, A. Smogunov, I. Timrov, T. Thonhauser, P. Umari, N. Vast, X. Wu, and S. Baroni, "Advanced capabilities for materials modelling with Quantum ESPRESSO," J. Phys.: Condens. Matter **29**, 465901 (2017).

[23] D. R. Hamann, "Optimized norm-conserving Vanderbilt pseudopotentials," Phys. Rev. B **88**, 085117 (2013).

[24] J. P. Perdew and Y. Wang, "Accurate and simple analytic representation of the electron-gas correlation energy," Phys. Rev. B **45**, 13244 (1992).

[25] X. Luo, Y. Zhao, J. Zhang, Q. Xiong, and S. Y. Quek, "Anomalous frequency trends in MoS_2 thin films attributed to surface effects," Phys. Rev. B **88**, 075320 (2013).

[26] A. Molina-Sánchez, K. Hummer, and L. Wirtz, "Vibrational and optical properties of MoS_2: From monolayer to bulk," Surf. Sci. Rep. **70**, 554–586 (2015).

[27] C. Rice, R. Young, R. Zan, U. Bangert, D. Wolverson, T. Georgiou, R. Jalil, and K. Novoselov, "Raman-scattering measurements and first-principles calculations of strain-induced phonon shifts in monolayer MoS_2," Phys. Rev. B **87**, 081307 (2013).

[28] L. Cartz and B. Tooper, "Dehydration of phlogopite micas studied by high-temperature transmission electron microscopy," J. Appl. Phys. **36**, 2783–2787 (1965).

[29] O. Ochedowski, B. K. Bussmann, and M. Schleberger, "Graphene on mica - intercalated water trapped for life," Sci. Rep. **4**, 6003 (2014).

[30] I. V. Markov, *Crystal Growth for Beginners*, 2nd ed. (World Scientific, 2003).

[31] C. Roland and G. H. Gilmer, "Epitaxy on surfaces vicinal to Si(001). I. Diffusion of silicon adatoms over the terraces," Phys. Rev. B **46**, 13428–13436 (1992).

[32] H. Brune, K. Bromann, H. Röder, K. Kern, J. Jacobsen, P. Stoltze, K. Jacobsen, and J. Norskov, "Effect of strain on surface diffusion and nucleation," Phys. Rev. B **52**, R14380–R14383 (1995).